Cross-receptive Focused Inference Network for Lightweight Image Super-Resolution

Wenjie Li, Juncheng Li, Guangwei Gao, *Senior Member, IEEE,* Jiantao Zhou, *Senior Member, IEEE,* Jian Yang, *Member, IEEE* and Guo-Jun Qi, *Fellow, IEEE*

***Abstract*—With the development of deep learning, single image super-resolution (SISR) has achieved significant breakthroughs. Recently, methods to enhance the performance of SISR networks based on global feature interactions have been proposed. However, the capabilities of neurons that need to adjust their function in response to the context dynamically are neglected. To address this issue, we propose a lightweight Cross-receptive Focused Inference Network (CFIN), a hybrid network composed of a Convolutional Neural Network (CNN) and a Transformer. Specifically, a novel Cross-receptive Field Guide Transformer (CFGT) is designed to adaptively modify the network weights by using modulated convolution kernels combined with local representative semantic information. In addition, a CNN-based Cross-scale Information Aggregation Module (CIAM) is proposed to make the model better focused on potentially practical information and improve the efficiency of the Transformer stage. Extensive experiments show that our proposed CFIN is a lightweight and efficient SISR model, which can achieve a good balance between computational cost and model performance.**

***Index Terms*—Cross-receptive, cross-attention, hybrid network, lightweight mode, SISR.**

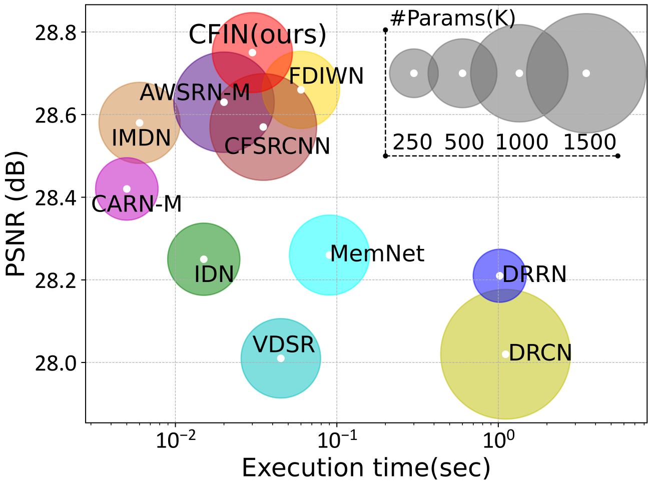

Fig. 1: Model inference time studies on Set14 (×4).

I. Introduction

The task of Single Image Super-Resolution (SISR) aims to estimate a realistic High-Resolution (HR) image from the Low-Resolution (LR) one, which plays a fundamental role in various computer vision tasks, including surveillance imaging, autonomous driving, and medical imaging [1]–[3]. As an ill-posed problem, SISR is still a challenging task. To solve this task, many Convolutional Neural Networks (CNN) based methods have been proposed to directly learn the mapping between the LR and HR image pairs. For example, Dong *et al.* presented the first CNN-based model, dubbed SRCNN [4]. Although SRCNN only has three convolutional layers, its performance is significantly better than traditional solutions. Subsequently, a series of networks with complex architectures were proposed, and deep CNN-based methods have achieved remarkable progress in SISR [5], [6]. Although these models have achieved promising results, their computational cost is often too huge (Fig. 1) to be popularized and widely used.

To solve the aforementioned problems, constructing lightweight SISR models has attracted more and more attention. Among these CNN-based lightweight models, most of them focus on efficient network architecture design, such as neural architecture search [7], multi-scale structure design [8], [9], and channel grouping strategy [10], [11]. However, convolution kernels can only extract local features, which is difficult to model the long-term dependencies of the image. As a complementary solution to CNN, Transformer has achieved excellent performance in many visual tasks with its powerful global modeling capability [12]–[15]. Recently, some Transformer-based SISR methods have been proposed [16]–[18]. For instance, SwinIR [19] introduced Transformer into SISR, relying on its advantage of using a shifted window scheme to model long-term dependencies, showing the great promise of Transformer in SISR. ESRT [20] is an efficient SISR model that combine a lightweight CNN and lightweight Transformer in an end-to-end model. However, most existing Transformer-based methods ignore the importance of dynamic modeling with context. As studied in neurology [21], the morphology of neurons should change adaptively with changes in the environment. This adjustment mechanism has been studied in many fields. For example, Jia *et al.* [22] gener-

Wenjie Li and Guangwei Gao are with the Institute of Advanced Technology, Nanjing University of Posts and Telecommunications, Nanjing, China, and also with the Key Laboratory of Intelligent Information Processing, Nanjing Xiaozhuang University, Nanjing, China (e-mail: csggao@gmail.com,lewj2408@gmail.com).

Juncheng Li is with the Center for Mathematical Artificial Intelligence, Department of Mathematics, The Chinese University of Hong Kong, Hong Kong, China (e-mail: cvjunchengli@gmail.com).

Jiantao Zhou is with the State Key Laboratory of Internet of Things for Smart City, University of Macau, Taipa, Macau, and also with the Department of Computer and Information Science, Faculty of Science and Technology, University of Macau, Taipa, Macau (e-mail: jtzhou@um.edu.mo).

Jian Yang is with the School of Computer Science and Technology, Nanjing University of Science and Technology, Nanjing, China (e-mail: csjyang@njust.edu.cn).

Guo-Jun Qi is with the Department of Computer Science, University of Central Florida, Orlando, USA (e-mail: guojunq@gmail.com).

ated convolution kernel weights from the features extracted from another network. Chen *et al.* [23] aggregated multiple convolution kernels in parallel and based on local attention to adaptively adjust the weights. Lin *et al.* [24] presented the context-gated convolution to incorporate context awareness into the convolutional layer.

Motivated by the above methods, in this paper, we introduce the power of contextual reasoning into Transformer and propose a lightweight Cross-receptive Focused Inference Network (CFIN) for SISR. CFIN is a hybrid network composed of a Convolutional Neural Network (CNN) and a Transformer. In the convolution stag, a Cross-scale Information Aggregation Module (CIAM) is designed to extract more potentially useful information with the help of the efficient Redundant Information Filter Unit (RIFU). In the Transformer stage, we propose an efficient Cross-receptive Field Guide Transformer (CFGT) to achieve cross-scale long-distance information fusion with the specially designed Context Guided Attention (CGA). In summary, the main contributions of this paper can be summarized as the following three aspects

- We propose a Redundant Information Filter Unit (RIFU), which can remove redundant information and accurately learn flexible local features. Meanwhile, an efficient Cross-scale Information Aggregation Module (CIAM) is specially designed for elaborately combining several RIFUs to ensure full use of local features.
- We propose a new Context Guided Attention (CGA) scheme, which can adaptively adjust the weights of the convolution kernel according to the representative local information in the context. In addition, a novel Cross-receptive Field Guide Transformer (CFGT) is proposed for cross-scale long-distance information fusion, which is more conducive to contextual reasoning within CGAs and suitable for long-distance modeling.
- We propose a lightweight and efficient Cross-receptive Focused Inference Network (CFIN) for SISR. CFIN elegantly integrates CNN and Transformer, achieving competitive performance and a good balance between computational cost and model performance.

The rest of this paper is organized as follows. Related works are reviewed in Section II. A detailed explanation of the proposed CFIN is given in Section III. The experimental results, ablation studies, and discussion are presented in Sections IV, V, and VI respectively. Finally, we draw a conclusion in Section VII.

II. Related Work

A. Lightweight SISR Method

Due to the powerful learning ability of CNN, more and more CNN-based potent SISR methods have been proposed. However, most of the methods are limited in real-world applications by their huge computational cost. To handle this issue, some lightweight and efficient SISR methods have been presented [17], [25]–[31]. For example, IDN [32] used an information distillation network to selectively fuse features, and then IMDN [33] improved it to build a lighter model. RFDN [34] combines channel splitting and residual structure to achieve better performance. IMRN [35] adopted the strategy of model pruning to alleviate the model size without significantly degrading the performance. FDIWN [36] improved the model performance by making full use of the intermediate layer features. However, most of these methods do not consider the influence of redundant features on model learning. Meanwhile, these CNN-based methods cannot observe images through global feature interaction. In this paper, we aim to explore a more efficient lightweight model that can focus on potentially practical information.

B. Context Reasoning

With the in-depth understanding of deep learning, researchers tentatively explored how to increase the contextual information of the model. It can be roughly divided into the following categories. For example, using the attention mechanism to modify the feature representation, and the typical one is to modify the local features through the attention mechanism [37]. However, most of them can only modify the features by changing the input mapping. Recently, some works [23], [38]–[40] try to dynamically change network parameters by analyzing local or global information. However, they only consider local fragments [38], ignore weight tensors in convolutional layers [39] or have high training costs [40]. Researchers in [41] imitated the human visual system and simulates the bottom-up impact of semantic information on the model through reverse connections, but this feedback mechanism is difficult to explain in the model. In addition, none of them use local contextual information to dynamically guide global attention interactions. In this work, we aim to introduce context reasoning to further enhance the performance of the model and build a model that can adaptively modify the network weights.

III. Proposed Method

A. Cross-receptive Focused Inference Network

In this paper, we devise a lightweight Cross-receptive Focused Inference Network (CFIN) for SISR. As shown in Fig. 2, CFIN consists of several CNN-Transformer (CT) blocks and two PixelShuffle layers. Meanwhile, each CT block contains a convolution stage and a Transformer stage. And each two CT blocks are called once using a loop mechanism for a better trade-off between model size and performance. We define the input and output of CFIN as I_{LR} and I_{SR}, respectively. Firstly, the dimension of the input image is rapidly increased to obtain shallow features $I_{shallow}$ for subsequent processing

$$I_{shallow} = F_{cr}(I_{LR}), \tag{1}$$

where $F_{cr}(\cdot)$ is the channel expansion operation. Then the shallow features are sent to the CT block for feature extraction and the complete operation of each CT block can be defined as follows

$$I^{i}_{ct} = F^{i}_{CT}(I^{i}_{in}) = F_{cr}(F_T(F_{ce}(F_C(I^{i}_{in})))) + I^{i}_{in}, \tag{2}$$

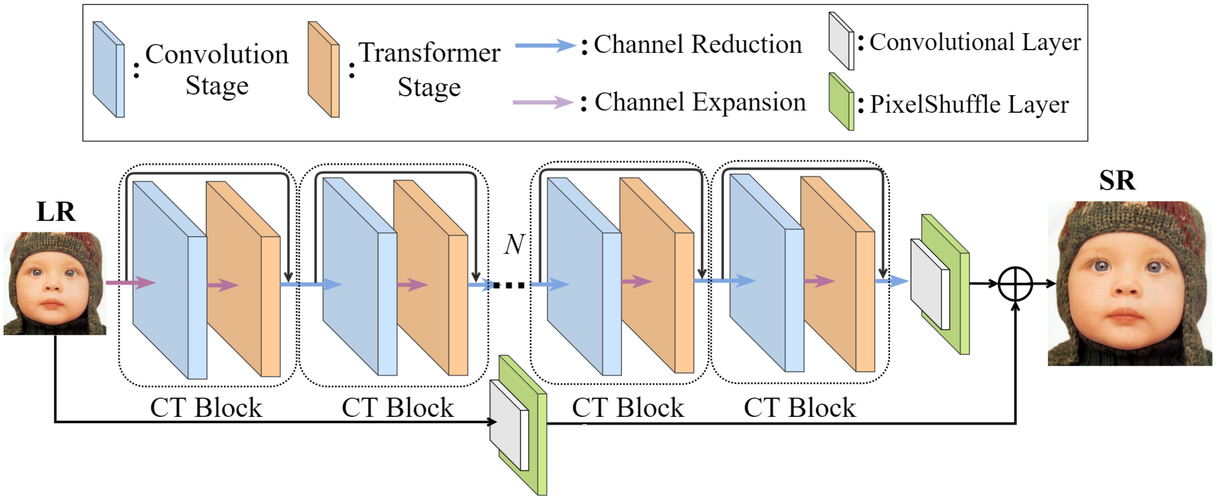

Fig. 2: The overall architecture of the proposed Cross-receptive Focused Inference Network (CFIN). It is worth noting that 1×1 convolution is used for channel reduction and channel expansion in CFIN.

where $F_{cr}(\cdot)$, $F_{ce}(\cdot)$, $F_C(\cdot)$, $F_F(\cdot)$ denote the channel reduction operation, channel expansion, the convolution stage, and the Transformer stage, respectively. I_{in}^i and I_{ct}^i are the input and output of the i-th CT block. After the operation of N CT blocks, we can attain the final deep features as

$$I_{ct} = F_{CT}(I_{shallow}) = F_{CT}^N(F_{CT}^{N-1}(\cdots F_{CT}^2(F_{CT}^1(I_{shallow})))), \tag{3}$$

where I_{ct} denotes the output of the N-th CT block. Finally, to obtain the final SR image, both I_{ct} and I_{LR} are simultaneously fed into the post-sampling reconstruction module

$$I_{SR} = F_{rec}(I_{ct}) + F_{rec}(I_{LR}), \tag{4}$$

where $F_{rec}(\cdot)$ is the post-sampling reconstruction module, which composed of a 3×3 convolutional layer and a PixelShuffle layer.

B. Convolution Stage

In the convolution stage, we propose a Cross-scale Information Aggregation Module (CIAM) to mine potential image information and make the model understand the preliminary SR information. As shown in Fig. 3, CIAM is mainly composed of three Redundant Information Filter Units (RIFU).

1) Redundant Information Filter Unit (RIFU): According to previous works [42], [43], we can know that it is easier to recover the smooth area that occupies most of the image area, but the complex texture information that occupies a small area of the image is difficult to recover. However, most SR methods tend to treat all areas of the image equally, which leads to the smooth area that accounts for most areas of the image being paid more attention by the network, which may miss the correct texture information, so accurate modeling cannot be achieved. In previous work [44], some methods convert the image from the time domain to the frequency domain by discrete cosine transform (DCT), and then manually set a threshold T to discard the frequency domain information greater or less than T to filter the secondary information. However, we also found that the input images used for training vary widely. Using manual thresholding is sensitive to noise, which is not suitable for all images. Therefore, we aim to explore a method that can make the network find a mask that instructs model pays more attention to texture features. To achieve this, we propose a Redundant Information Filter Unit (RIFU). As given in Fig. 3, after the input feature x enters RIFU, it first goes through a convolutional layer and an activation layer to obtain a mixed feature X. Then, we use a 1×1 convolutional layer to transform the number of channels of the output R to M ($M = 3$) and its process can be formulated as

$$X = f_{lrelu}(f_{conv}^{3x3}(x)), \tag{5}$$

$$R = f_{n->3}(X), \tag{6}$$

where $f_{conv}^{3x3}(\cdot)$ represents the 3×3 convolutional layer, $f_{lrelu}\cdot$ represents the LeakyRelu function, and $f_{n->3}$ represents the 1×1 convolutional layer. Next, in order to complete the end-to-end network optimization, we use the Gumbel Softmax trick [45] to generate a continuous differentiable normal distribution, which can well approximate the probability distribution represented by the network output and randomly add some sampling, so the Gumbel-Softmax enables RIFU to retain some potentially useful information in addition to salient features. It's process can be formulated as follows

$$GS_i = \frac{\exp((R_i + gs_i)/\tau)}{\sum_{m=1}^{M} \exp((R_{i_m} + gs_{i_m})/\tau)}, \tag{7}$$

where τ defaults to 1, and gs_i represents the noise obeying the $Gumbel(0,1)$ distribution. During training we need model to select only one channel from the three channels and the channel selection formula is as follows

$$y_{mask} = \arg one(GS_{i_m}), \tag{8}$$

where y_{mask} represents the single-channel output feature after masking, and $\arg one(.)$ represents the argmax branch of GS_i in m channels. After that, we multiply X by the y_{mask} feature

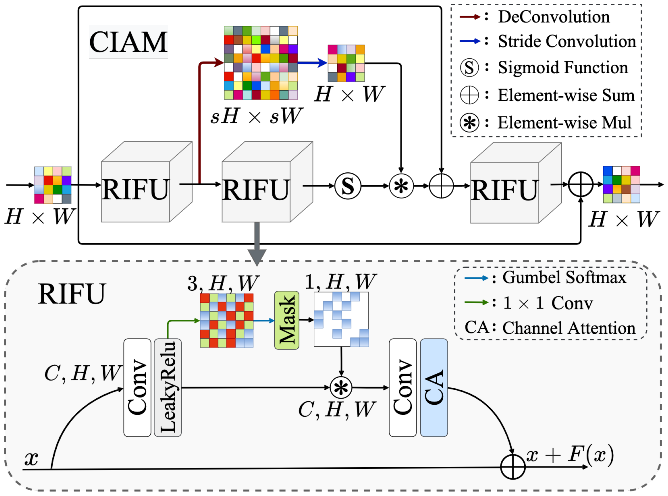

Fig. 3: The framework of the designed Cross-scale Information Aggregation Module (CIAM) and Redundant Information Filter Unit (RIFU).

mask to preserve the initial details, and get the finally output y of RIFU through residual connection

$$y = f_{CA}(f_{conv}^{3x3}(y_{mask} \times X)) + x, \tag{9}$$

where $f_{CA}(\cdot)$ represents the channel attention mechanism.

2) Cross-scale Information Aggregation Module (CIAM): Due to the difference in model structure, it is inevitable that the learned features are redundant. Meanwhile, with limited computing resources, we hope that the model will pay more attention to features with higher priority. So CIAM is designed to efficiently combine RIFU, its role is to extract more potentially effective information, mine deep image features, and make full use of information from different scales to observe image features.

In terms of network architecture design, simply combining RIFU in series is not conducive to gradient flow and collecting contextual information at different spatial locations. To solve this problem, we innovatively use two different scale spaces for feature transformation in the middle of the module. Among them, one is the original space, whose feature map size has the same resolution as the input, and the other is the large space after deconvolution operation. The receptive field of the transformed embedding is very large and can be used to guide the feature transformation in the original feature map. The process can be defined as

$$x_{HW}^1 = f_{RIFU}(x_{HW}), \tag{10}$$

$$x_{HW}^2 = f_{sconv}(f_{deconv}(x_{HW})) \times f_{sig}(f_{RIFU}(x_{HW}^1)), \tag{11}$$

where x_{HW}^i represents the output features with the size of $H \times W$ after the i-th LFFU, $f_{RIFU}(\cdot)$ represents the proposed LFFU, $f_{sconv}(\cdot)$ and $f_{deconv}(\cdot)$ represent the deconvolution and strided convolution with $s = 2$, and $f_{sig}(\cdot)$ represents the Sigmoid function.

Finally, to prevent the vanishing gradient, the dense residual learning mechanism is introduced into the module. Therefore, this module has the potential for multiple RIFUs permutations and combinations, and its output x_{HW}^3 can be formulated as

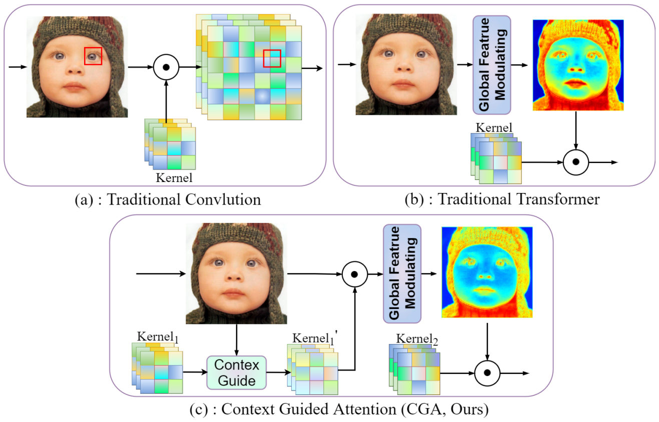
Kernel
(a) : Traditional Convlution
Global Featrue Modulating
Kernel
(b) : Traditional Transformer
Kernel$_1$
Contex Guide
Kernel$_1$'
Global Featrue Modulating
Kernel$_2$
(c) : Context Guided Attention (CGA, Ours)

Fig. 4: (a) Traditional convolution tends to focus on local features. (b) Traditional Transformer uses global feature interactions to focus on key information. (c) Our proposed Context Guided Attention (CGA), guided by locally representative modulated convolution kernels, is able to adaptively combine global information to modify feature maps. $\odot$ denotes the convolution operation.

$$x_{HW}^3 = f_{RIFU}(x_{HW}^2 + x_{HW}^1) + x_{HW}. \tag{12}$$

C. Transformer Stage

In recent years, Transformer has shown great potential on SISR, which can learn global information of images through its powerful self-attention mechanism. However, existing self-attention mechanisms often neglect to incorporate context and build attention across features at different scales. To address this issue, in the Transformer stage, we propose a Cross-receptive Field Guided Transformer (CFGT). In CFGT, a specially designed Context Guided MaxConv (CGM) is introduced as its basic unit, which can provide cross-features for the model across scales. Meanwhile, it can adaptively adjust the weights of the network through semantic reasoning to meet the requirements of long-distance modeling.

1) Context Guided Attention (CGA): As shown in Fig. 4, traditional convolution tends to focus on local features and traditional Transformer uses self-attention to capture the global Information. However, the traditional Transformer cannot take into account the locally representative dominant features, and the self-attention mechanism also unable to incorporate contextual semantic information. To alleviate this problem, we propose a new attention, named Context Guided Attention (CGA), which is guided by the locally representative modulated convolution kernels and can adaptively combine global information to modify feature maps.

According to Fig. 5, we can clearly see that before computing the feature covariance to generate the global attention map, we introduce the Context Guided MaxConv (CGM) to emphasize the local context. Specifically, we first generate query (Q), key (K), and value (V) projections from the input tensor $X \in \Re^{C \times H \times W}$. After that, we separately add

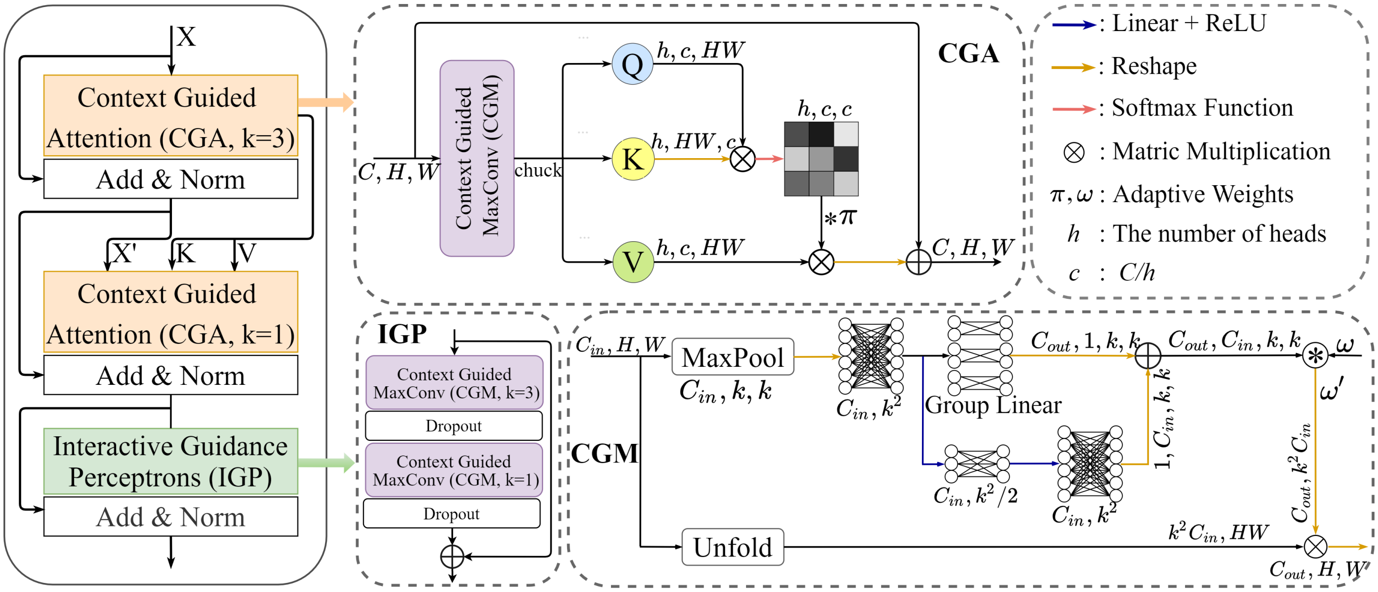

Fig. 5: The architecture of the proposed Cross-receptive Field Guide Transformer (CFGT), Context Guided Attention (CGA), Context Guided MaxConv (CGM), and Interactive Guidance Perceptrons (IGP).

representative local contexts to them, which are obtained by encoding the channel context through CGM $Q = W^{Q}_{CGM}(X)$, $K = W^{K}_{CGM}(X)$, and $V = W^{V}_{CGM}(X)$, $(Q, K, V) \in \Re^{h \times C/h \times HW}$. Among them, h is the amount of attention and $W_{CGM}(\cdot)$ represents the proposed CGM, similar to traditional multi-head attention [46]. In this work, we divide the number of channels into h groups for parallel learning, and the size of Q, K, V is obtained after reshaping the tensor from the input image. Finally, we take the dot-product to reshape the Q and V projections to generate a transposed attention map of size $\Re^{h \times C/h \times C/h}$ instead of a regular feature map of size $\Re^{h \times HW \times HW}$ [47]. Overall, the attention mechanism in CGA can be formulated as

$$\underset{CGA}{Att}(Q, K, V) = V \cdot Soft((K \cdot Q)/\omega), \tag{13}$$

where $Soft(\cdot)$ represents the Softmax function, $\cdot$ represents the dot product operation, ω represents a learnable adaptive parameter. Due to the powerful function of CGM combined with local features to explicitly modify the modulation kernel, the projection vector generated in the previous space can be used to guide the generation of subsequent attention.

Context Guided MaxConv (CGM). Recently, methods for contextual reasoning [48], [49] have been extensively studied in computer vision. Motivated by [24], we propose a Context Guided MaxConv (CGM) to dynamically extract representative local patterns within Transformer in conjunction with contextual guidance. As shown in Fig. 5, to extract the most representative information, we scale the input image to the size of $k \times k$ by using the max-pooling operation. Then, to alleviate the time-consuming kernel modulation caused by a large number of channels, we follow the previous idea and reduce the complexity by generating two tensors through two branches. One of the branches draws on the idea of bottleneck design [37]. We project the spatial position information into a vector of size k through a linear layer of shared parameters and then generate new channel weights from this vector. In another branch, the idea of grouped convolution is applied to the linear layer, and the output C_{out} is obtained by introducing a grouped linear layer with weight ($w \in \Re^{\frac{C_{in}}{g} \times \frac{C_{out}}{g}}$), where g is the number of groups. Then, spatially transformer the two branches to obtain tensors with corresponding sizes of $C_{out}, 1, k, k$ and $C_{in}, 1, k, k$. Meanwhile, the two tensors are then added element-wise to get the same size as the convolution kernel $\omega (\omega \in \Re^{C_{out} \times C_{out} \times k \times k})$, which is convenient for element-wise multiplication to obtain the modulation convolution kernel. It's worth to noting that ω is an adaptive multipliers that is consistent with the size of the tensor. After multiplying(*) it with the tensor, the tensor can be converted into a set of trainable type parameters and bound to the module. During the learning process, the weights of ω can be automatically learned and modified to optimize the model. After that, the two tensors are added element by element to obtain the same size as the convolution kernel ω, which is convenient for element-wise multiplication to obtain the modulation convolution kernel ω'. Finally, after fully understanding the obtained semantic information, this set of optimized tensor ω' interacts with the input features to dynamically capture the local patterns of salient features.

2) Cross-receptive Field Guide Transformer (CFGT): In this paper, we propose a Cross-receptive Field Guide Transformer (CFGT) for long-distance modeling. As shown in Fig. 5, CFGT is mainly composed of two CGAs and one Interactive Guidance Perceptrons (IGP) in the encoder part of CFGT. Meanwhile, hierarchical normalization is performed after each block and the local residual connection is used. It is worth noting that the CGM in the two CGAs adopts different k (k represents the size of the receptive field that the CGM focuses on). Therefore, cross-attention can supplement the model with cross-scale features. We assume that the input of CFGT is T_{in}, then the output T_{out} can be formulated as

$$T_{med}^{1} = Norm(CGA(T_{in})) + T_{in}, \tag{14}$$

$$T_{med}^{2} = Norm(CGA(T_{in}, K, V)) + T_{med1}, \tag{15}$$

$$T_{out} = Norm(IGP(T_{med2})) + T_{med2}, \tag{16}$$

where K and V are the key and value generated by the first CGA, **and they will serve as part of the input of the second CGA**. The operation of the second CGA can be defined as

$$\underset{CGA}{Att}(Q', K', V') = (V'+V)\cdot Soft(((K'+K)\cdot Q')/\omega). \tag{17}$$

Similarly, our IGP also adopts the idea of cross receptive fields, connecting a CGM with $k = 3$ and a CGM with $k = 1$ using a residual structure to enhance attention of the transformer.

D. Loss Function

During training, given a training set $\{I_i^{LR}, I_i^{HR}\}_{i=1}^{N}$, the loss function of CFIN can be expressed by

$$Loss\,(\theta) = \arg\min_{\theta} \frac{1}{N}\sum_{i=1}^{N} \left\| F_{CFIN}(I_{LR}^{i}) - I_{HR}^{i} \right\|_1, \tag{18}$$

where $F_{CFIN}(\cdot)$ represent our proposed CFIN, θ represent the parameter set of CFIN, N represent the number of LR-HR pairs in the training set.

IV. Experiments

In this part, we provide relevant experimental details, descriptions, and results to verify the effectiveness and excellence of the proposed CFIN.

A. Datasets and Metrics

Following previous works, we utilize DIV2K [57] (1-800) as our training dataset. Meanwhile, we used five benchmark datasets to verify the effectiveness of the proposed model, including Set5 [58], Set14 [59], BSDS100 [60], Urban100 [61], and Manga109 [62]. Additionally, we used Peak Signal-to-Noise Ratio (PSNR) and Structural Similarity (SSIM) to evaluate the quality of our restored images on the Y channel of the YCbCr color space.

B. Implementation Details

During training, we randomly crop patches with the size of 48×48 from the training set as input and use horizontal flipping and random rotation for data augmentation. The initial learning rate is set to 5×10^{-4}, which is finally reduced to 6.25×10^{-6} by cosine annealing. Meanwhile, we implement our model with the PyTorch framework and update it with Adam optimizer. All our experiments are conducted on NVIDIA RTX 2080Ti GPU. In the final model, we use 8 transformer stages and 8 convolution stages, and all of which are called twice using a loop mechanism. Meanwhile, we set the initial input channel to 48 and use the weight normalization [63] after each convolutional layer in RIFUs.

C. Comparison with Advanced Lightweight SISR Models

In this section, we compare our proposed CFIN with other advanced lightweight SISR models to verify the effectiveness of the proposed model. In TABLE I, we compare CFIN with CNN-based models. From the table, we can clearly observe that our CFIN+ and CFIN stand out from these methods and achieve the best and the second best results on almost all datasets. It is worth mentioning that our CFIN consumes less parameters and computation than most methods. This benefit from the well-designed CNN and Transformer in CFIN, which can efficiently extract the local features and integrate the global information of the image. To further demonstrate the superiority of CFIN, in TABLE II, we also provide a comprehensive comparison with some advanced Transformer-based models, including the lightweight version of SwinIR* [19], ESRT [20], and LBNet [17]. All these models are the most advanced lightweight SISR models. From the table, we can see that our CFIN achieves better results than ESRT and LBNet with fewer parameters. Compared with SwinIR*, our CFIN can still achieve close results than it with fewer parameters, Multi-adds, and execution time. It is worth mentioning that SwinIR* uses a pre-trained model for initialization, and setting the patch size as 64×64 during training. Extensive experiments have shown that the larger the patch size, the better the results. Meanwhile, some previous works [9], [64] have pointed out that the performance of models trained with multiple upsampling factors shows better results than the single one since using the inter-scale correlation between different upsampling factors can improve the model performance. Therefore, these methods can further improve the model performance. Moreover, we provide the results of the large version of CFIN, donated as CFIN-L. It can be seen that the results of CFIN-L even surpass SwinIR* on some datasets and still keep fewer parameters and less time. This is due to the rational structural design and strong modeling capabilities of CFIN. All these results fully illustrate the strong competitiveness of CFIN in balancing model size and performance.

In addition, we also provide a visual comparison of CFIN with other SISR methods in Fig. 6. Obviously, our CFIN can reconstruct high-quality images with more accurate textures details and edges. This further demonstrate the effectiveness of the proposed CFIN.

V. Ablation Studies

In this section, we provide a series of ablation studies to further demonstrate the effectiveness of the proposed modules and model.

A. Network Investigations

1) The effectiveness of RIFU: In RIFU, we use feature masks to remove redundant features. To study and verify the effectiveness of this mechanism, we remove the mask and provide the results in TABLE III. According to the table, we can see that the PSNR value increases by 0.08dB after using the masking mechanism under the slight increase in the number of parameters.

TABLE I: Average PSNR/SSIM comparison with other advance CNN-based SISR models. The Best and the second best results are highlighted and underlined, respectively. '+' indicates that the model uses a self-ensemble strategy.

Method	Scale	Params	Multi-adds	Set5	Set14	BSDS100	Urban100	Manga109
				PSNR/SSIM	PSNR/SSIM	PSNR/SSIM	PSNR/SSIM	PSNR/SSIM
MemNet [50]	×2	677K	-	37.78/0.9597	33.28/0.9142	32.08/0.8978	31.31/0.9195	-
IDN [32]		553K	124.6G	37.83/0.9600	33.30/0.9148	32.08/0.8985	31.27/0.9196	38.01/0.9749
CARN [10]		1592K	222.8G	37.76/0.9590	33.52/0.9166	32.09/0.8978	31.92/0.9256	38.36/0.9765
IMDN [33]		694K	158.8G	38.00/0.9605	33.63/0.9177	32.19/0.8996	32.17/0.9283	38.88/0.9774
AWSRN-M [51]		1063K	244.1G	38.04/0.9605	33.66/0.9181	32.21/ 0.9000	32.23/0.9294	38.66/0.9772
MADNet [26]		878K	187.1G	37.85/0.9600	33.38/0.9161	32.04/0.8979	31.62/0.9233	-
MAFFSRN-L [52]		790K	154.4G	38.07/0.9607	33.59/0.9177	32.23/0.9005	32.38/0.9308	-
LAPAR-A [53]		548K	171.0G	38.01/0.9605	33.62/0.9183	32.19/0.8999	32.10/0.9283	38.67/0.9772
GLADSR [27]		812K	187.2G	37.99/0.9608	33.63/0.9179	32.16/0.8996	32.16/0.9283	-
LatticeNet+ [54]		756K	165.5G	38.15/0.9610	33.78/0.9193	32.25/0.9005	32.43/0.9302	-
DCDN [55]		756K	-	38.01/0.9606	33.52/0.9166	32.17/0.8996	32.16/0.9283	38.70/0.9773
SMSR [28]		985K	351.5G	38.00/0.9601	33.64/0.9179	32.17/0.8990	32.19/0.9284	38.76/0.9771
ECBSR [56]		596K	137.3G	37.90/0.9615	33.34/0.9178	32.10/0.9018	31.71/0.9250	-
PFFN [29]		569K	138.3G	38.07/0.9607	33.69/0.9192	32.21/0.8997	32.33/0.9298	38.89/0.9775
DRSAN [30]		690K	159.3G	38.11/0.9609	33.64/0.9185	32.21/0.9005	32.35/0.9304	-
FDIWN [36]		629K	112.0G	38.07/0.9608	33.75/0.9201	32.23/0.9003	32.40/0.9305	38.85/0.9774
CFIN (Ours)		675K	116.9G	38.14/ 0.9610	33.80/0.9199	32.26/ 0.9006	32.48/ 0.9311	38.91/0.9770
CFIN+ (Ours)		675K	116.9G	**38.22/ 0.9613**	**34.01/ 0.9221**	**32.35/ 0.9016**	**32.93/ 0.9347**	**39.21/ 0.9777**
MemNet [50]	×3	677K	-	34.07/0.9248	30.00/0.8350	28.96/0.8001	27.56/0.8376	-
IDN [32]		553K	56.3G	34.11/0.9253	29.99/0.8354	28.95/0.8013	27.42/0.8359	32.71/0.9381
CARN [10]		1592K	118.8G	34.29/0.9255	30.29/0.8407	29.06/0.8034	28.06/0.8493	33.43/0.9427
IMDN [33]		703K	71.5G	34.36/0.9270	30.32/0.8417	29.09/0.8046	28.17/0.8519	33.61/0.9445
AWSRN-M [51]		1143K	116.6G	34.42/0.9275	30.32/0.8419	29.13/0.8059	28.26/0.8545	33.64/0.9450
MADNet [26]		930K	88.4G	34.16/0.9253	30.21/0.8398	28.98/0.8023	27.77/0.8439	-
MAFFSRN-L [52]		807K	68.5G	34.45/0.9277	30.40/0.8432	29.13/0.8061	28.26/0.8552	-
LAPAR-A [53]		594K	114.0G	34.36/0.9267	30.34/0.8421	29.11/0.8054	28.15/0.8523	33.51/0.9441
GLADSR [27]		821K	88.2G	34.41/0.9272	30.37/0.8418	29.08/0.8050	28.24/0.8537	-
LatticeNet+ [54]		765K	76.3G	34.53/0.9281	30.39/0.8424	29.15/0.8059	28.33/0.8538	-
DCDN [55]		765K	-	34.41/0.9273	30.31/0.8417	29.08/0.8045	28.17/0.8520	33.54/0.9441
SMSR [28]		993K	156.8G	34.40/0.9270	30.33/0.8412	29.10/0.8050	28.25/0.8536	33.68/0.9445
PFFN [29]		558K	69.1G	34.54/0.9282	30.42/0.8435	29.17/0.8062	28.37/0.8566	33.63/0.9455
EMASRN+ [31]		427K	-	34.48/0.9275	30.38/0.8422	29.11/0.8046	28.17/0.8514	33.71/0.9450
DRSAN [30]		740K	76.0G	34.50/0.9278	30.39/0.8437	29.13/0.8065	28.35/0.8566	-
FDIWN [36]		645K	51.5G	34.52/0.9281	30.42/0.8438	29.14/0.8065	28.36/0.8567	33.77/0.9456
CFIN (Ours)		681K	53.5G	34.65/ 0.9289	30.45/ 0.8443	29.18/ 0.8071	28.49/ 0.8583	33.89/ 0.9464
CFIN+ (Ours)		681K	53.5G	**34.75/0.9298**	**30.59/0.8467**	**29.27/0.8091**	**28.85/0.8645**	**34.26/0.9484**
MemNet [50]	×4	677K	-	31.74/0.8893	28.26/0.7723	27.40/0.7281	25.50/0.7630	-
IDN [32]		553K	32.3G	31.82/0.8903	28.25/0.7730	27.41/0.7297	25.41/0.7632	29.41/0.8942
CARN [10]		1592K	90.9G	32.13/0.8937	28.60/0.7806	27.58/0.7349	26.07/0.7837	30.42/0.9070
IMDN [33]		715K	40.9G	32.21/0.8948	28.58/0.7811	27.56/0.7353	26.04/0.7838	30.45/0.9075
AWSRN-M [51]		1254K	72.0G	32.21/0.8954	28.65/0.7832	27.60/0.7368	26.15/0.7884	30.56/0.9093
MADNet [26]		1002K	54.1G	31.95/0.8917	28.44/0.7780	27.47/0.7327	25.76/0.7746	-
MAFFSRN-L [52]		830K	38.6G	32.20/0.8953	28.62/0.7822	27.59/0.7370	26.16/0.7887	-
LAPAR-A [53]		659K	94.0G	32.15/0.8944	28.61/0.7818	27.61/0.7366	26.14/0.7871	30.42/0.9074
GLADSR [27]		826K	52.6G	32.14/0.8940	28.62/0.7813	27.59/0.7361	26.12/0.7851	-
LatticeNet+ [54]		777K	43.6G	32.30/0.8962	28.68/0.7830	27.62/0.7367	26.25/0.7873	-
DCDN [55]		777K	-	32.21/0.8949	28.57/0.7807	27.55/0.7356	26.09/0.7855	30.41/0.9072
SMSR [28]		1006K	89.1G	32.12/0.8932	28.55/0.7808	27.55/0.7351	26.11/0.7868	30.54/0.9085
ECBSR [56]		603K	34.7G	31.92/0.8946	28.34/0.7817	27.48/0.7393	25.81/0.7773	-
PFFN [29]		569K	45.1G	32.36/0.8967	28.68/0.7827	27.63/0.7370	26.26/0.7904	30.50/0.9100
EMASRN+ [31]		546K	-	32.31/0.8964	28.66/0.7828	27.61/0.7364	26.15/0.7868	30.69/0.9105
DRSAN [30]		730K	49.0G	32.30/0.8954	28.66/0.7838	27.61/0.7381	26.26/0.7920	-
FDIWN [36]		664K	28.4G	32.23/0.8955	28.66/0.7829	27.62/0.7380	26.28/0.7919	30.63/0.9098
CFIN (Ours)		699K	31.2G	32.49/0.8985	28.74/0.7849	27.68/0.7396	26.39/0.7946	30.73/0.9124
CFIN+ (Ours)		699K	31.2G	**32.60/0.8998**	**28.86/0.7871**	**27.76/0.7419**	**26.71/0.8028**	**31.15/0.9163**

As we know, the max-pooling operation can filter redundant features and softmax can predict the probability distribution of different features. These functions also can make the model focus on the main features. To prove the effectiveness of the Gumbel-Softmax in RIFU, we replace the Gumbel-Softmax function with the max-pooling operation and softmax function, respectively. According to TABLE IV, we can see that the performance of the models will drop from 31.75dB to 31.71dB when only using the softmax function, and the performance will drop to 31.70dB when using the max-pooling operation. Therefore, we choose the Gumbel-Softmax operation in the final model. All the above experiments verify the effectiveness and necessity of each mechanism in RIFU.

2) The effectiveness of CIAM: To verify the effectiveness of CIAM, we replace CIAM with some commonly used feature extraction blocks in lightweight SISR models. It is worth noting that we remove the Transformer stage in each CT block to speed up the training. According to TABLE V, we can found that when the model uses CIAM for feature extraction, the parameter increase does not exceed 30K, Multi-

TABLE II: Comparison with some Transformer-base methods for ×4 SR. * means this model is pre-trained based on the ×2 setup and the training patch size is set to 64 × 64 (ours is 48 × 48 and without pre-training).

Method	Params	Multi-adds	GPU Memory	Time	Set5	Set14	BSD100	Urban100	Manga109	Average
					PSNR / SSIM	PSNR / SSIM	PSNR / SSIM	PSNR / SSIM	PSNR / SSIM	PSNR / SSIM
SwinIR* [19]	897K	49.6G	10500M	0.046s	32.44 / 0.8976	**28.77** / **0.7858**	**27.69** / **0.7406**	26.47 / **0.7980**	**30.92** / **0.9151**	29.26 / **0.8274**
ESRT [20]	751K	67.7G	4191M	0.032s	32.19 / 0.8947	28.69 / 0.7833	**27.69** / 0.7379	26.39 / 0.7962	30.75 / 0.9100	29.14 / 0.8244
LBNet [17]	742K	38.9G	6417M	0.043s	32.29 / 0.8960	28.68 / 0.7832	27.62 / 0.7382	26.27 / 0.7906	30.76 / 0.9111	29.12 / 0.8238
CFIN	699K	31.2G	11419M	0.035s	32.49 / 0.8985	28.74 / 0.7849	27.68 / 0.7396	26.39 / 0.7946	30.73 / 0.9124	29.21 / 0.8260
CFIN-L	852K	37.8G	14585M	0.040s	**32.56** / **0.8988**	28.74 / 0.7852	**27.69** / **0.7406**	**26.49** / 0.7973	30.85 / 0.9134	**29.27** / 0.8271

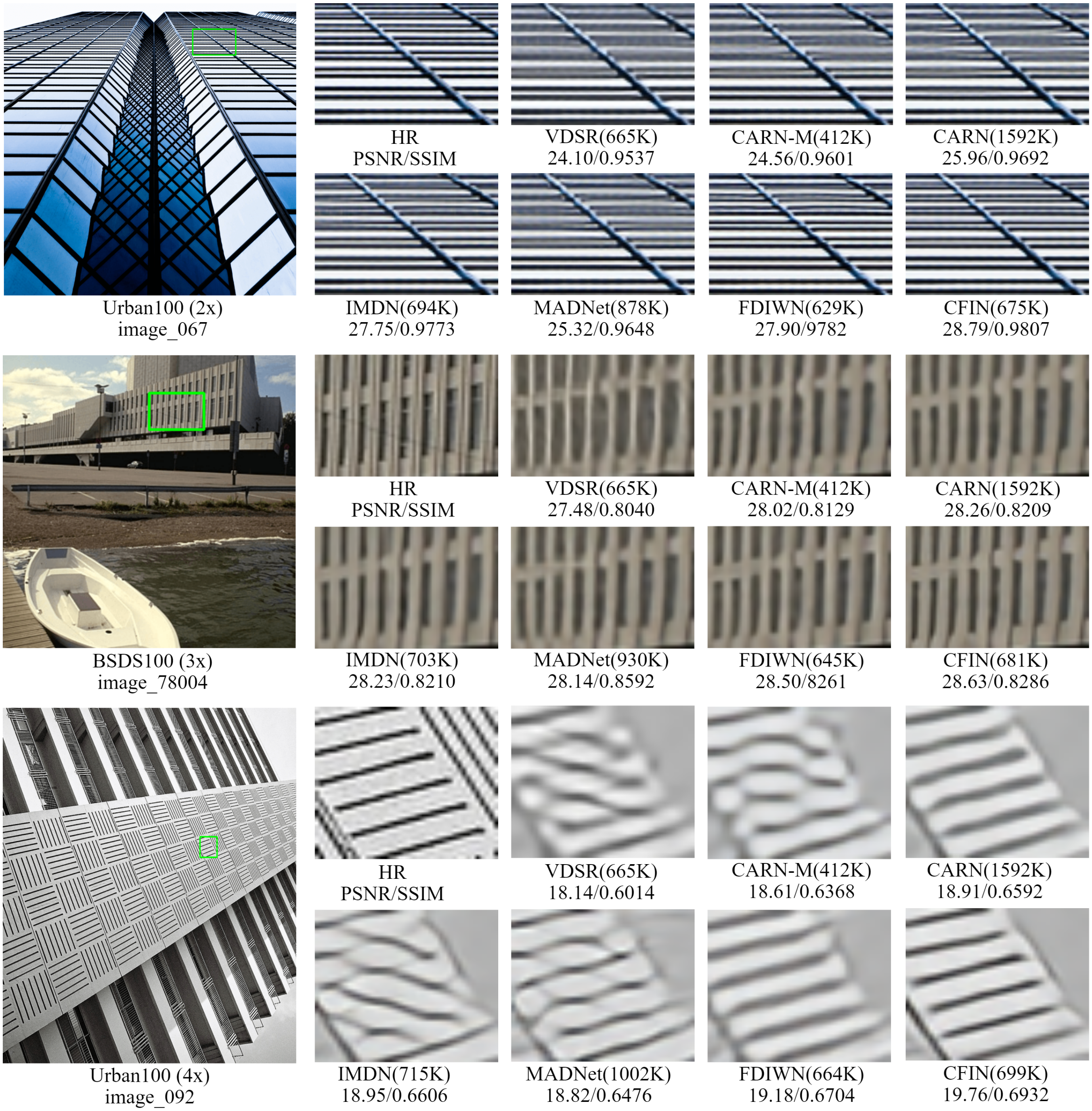

Fig. 6: Visual comparison with different lightweight SISR models. Obviously, our CFIN can reconstruct high-quality images.

TABLE III: Evaluate the effectiveness of masking mechanism.

Scale	Mask	Params	Multi-adds	Set14
				PSNR / SSIM
×4	✗	186.8K	6.18220G	28.22 / 07723
	✓	187.9K	6.21538G	**28.30 / 0.7738**

TABLE IV: Evaluate the effectiveness of Gumbel-Softmax.

Scale	Module	Params	Multi-adds	Set5
				PSNR / SSIM
×4	RIFU+Maxpool	165K	4.89G	31.70 / 0.8876
	RIFU+Softmax	165K	4.89G	31.71 / 0.8877
	RIFU+Gumbel-Softmax	165K	4.89G	**31.75 / 0.8886**

adds is less than most methods, but the model achieves the best results. This fully demonstrates the effectiveness of the proposed CIAM.

It is worth noting that the upsampling-downsampling branch in CIAM is also extremely important. Specifically, the performance (×4, Set5) of the ablation model (165K) with and without the upsampling-downsampling branch is 31.75dB and 31.63dB, respectively. But the position of this branch will not have much impact on model performance.

TABLE V: Evaluate the effectiveness of CIAM.

Module	Params	Multi-adds	Set5	Set14	U100
CFIN+RCAB [65]	192K	17.35G	31.63	28.19	25.29
CFIN+IMDB [33]	148K	8.47G	31.54	28.19	25.23
CFIN+RFDB [34]	140K	7.77G	31.68	28.26	25.34
CFIN+LB [54]	145K	8.16G	31.66	28.22	25.33
CFIN+HPB [20]	150K	8.91G	31.59	28.21	25.32
CFIN+WDIB [36]	147K	5.26G	31.68	28.26	25.37
CFIN+CIAM (Ours)	188K	6.22G	**31.87**	**28.30**	**25.44**

3) The effectiveness of CGM: Context Guided MaxConv is the basic unit in our Transformer stage, which is responsible for reasoning and guiding the entire network. To verify its importance, we replace CGM with the linear layer and group convolution, respectively. Meanwhile, we set their parameters as close as possible. According to TABLE VI, we can see that our CGM achieves better performance with fewer parameters and Multi-adds. This validates the excellence and effectiveness of the proposed CGM.

TABLE VI: Evaluate the effectiveness of CGM.

Module	Params	Multi-adds	Set5	B100	U100
CFIN+GConv	197K	5.7981G	31.95	27.41	25.68
CFIN+Linear	198K	4.1104G	29.19	26.37	23.62
CFIN+CGM (Ours)	178K	4.1105G	**32.14**	**27.43**	**25.71**

4) The effectiveness of CFGT: Compared with traditional Transformer, CFGT has two main differences in structure: the first is K, V for context communication; the second is cross-scale information exchange brought by CGM with different receptive fields. To assess the effectiveness of such a design, we provide a set of ablation experiments in TABLE VII, where **KV** stands for the contextual communication mechanism and **Cross** stands for the cross receptive fields mechanism. It can be seen that our architectural design solution can significantly improve the performance of the model with almost no additional computational cost. This validates the effectiveness of the proposed CFGT, which can better convey context.

TABLE VII: Evaluate the effectiveness of CFGT.

Scale	KV	Cross	Params	Multi-adds	Set5
					PSNR / SSIM
×4	✗	✓	177.8K	4.1105G	32.05 / 0.8928
	✓	✗	177.5K	4.1104G	31.93 / 0.8904
	✓	✓	177.8K	4.1105G	**32.14 / 0.8940**

Meanwhile, to verify that CFGT can effectively adjust attention according to the context, we make an efficiency trade-off on the number of CFGTs. In TABLE VIII, CFGT-N indicates that N CFGTs are used in the model. It can be seen that our model achieves more than 0.4dB improvement on the Manga109 at the cost of less than 70K parameters compared to the model without CFGT. In addition, we present the visual heatmap of different numbers of CFGTs in Fig. 7. Among them, the color close to red in the image represents the part where the attention is focused. So we can see that in the absence of CFGT, the attention is only focused on a small number of texture features, and as the number of CFGTs increases, more fine-grained features in images are paid attention to. This means that more CFGT makes the model tends to recover more accurate detailed features, which is conducive to image restoration.

TABLE VIII: Efficiency trade-off of CFGT.

Module	Params	Multi-adds	Set5	Manga109	Memory
CFGT-0	630K	28.0G	32.11	30.29	3551M
CFGT-4	665K	29.6G	32.27	30.49	7485M
CFGT-8	699K	31.2G	**32.49**	**30.73**	11419M

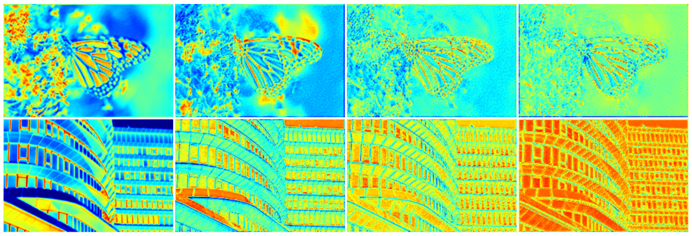
No CFGT 2 CFGTs 4 CFGTs 8 CFGTs

Fig. 7: The effect of CFGT on visual activation maps.

In TABLE IX, OnlyT indicates that only the Transformer part of the CFIN is retained. Compared with other advanced lightweight SISR models, it can be seen that our CFGT achieves promising results with only 91K parameters. This further verifies the effectiveness and advancement of CFIN.

TABLE IX: Comparison of CFGT with other methods.

Module	Params	Multi-adds	Set5	Set14	B100	U100
PAN [66]	272K	28.2G	32.13	28.61	**27.59**	**26.11**
MAFFSRN [52]	441K	19.3G	32.18	28.58	27.57	26.04
RFDN [34]	550K	31.6G	32.24	28.61	27.57	26.11
FDIWN-M [36]	454K	19.6G	32.17	28.55	27.58	26.02
OnlyT (Ours)	91K	4.5G	**32.33**	**28.61**	27.58	26.08

TABLE X: Evaluate the feasibility of combining CNN with Transformer.

Scale	Method	Params	GPU Memory	Time	Set5	Set14	BSD100	Urban100	Manga109
					PSNR / SSIM	PSNR / SSIM	PSNR / SSIM	PSNR / SSIM	PSNR / SSIM
×4	Pure-CNN	720K	3845M	0.016s	32.12 / 0.8939	28.52 / 0.7796	27.52 / 0.7343	25.96 / 0.7810	30.29 / 0.9057
	Pure-Transformer	94K	11549M	0.038s	32.48 / 0.8980	28.69 / 0.7835	27.64 / 0.7385	26.24 / 0.7896	30.62 / 0.9102
	CFIN (Ours)	699K	11419M	0.035s	**32.49 / 0.8985**	**28.74 / 0.7849**	**27.68 / 0.7396**	**26.39 / 0.7946**	**30.73 / 0.9124**

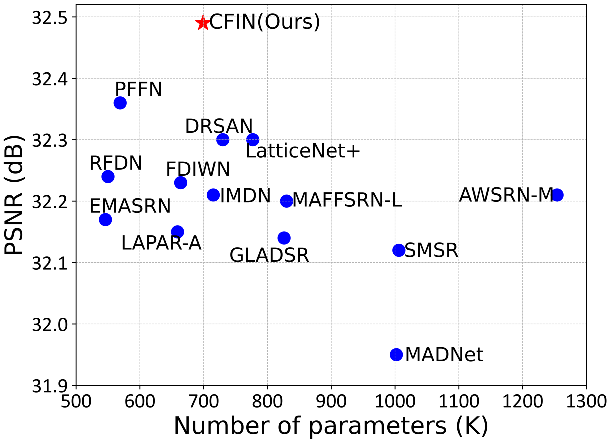

Fig. 8: Model performance and size comparison on Set5 (×4). Obviously, our CFIN achieves the best balance between model performance and size.

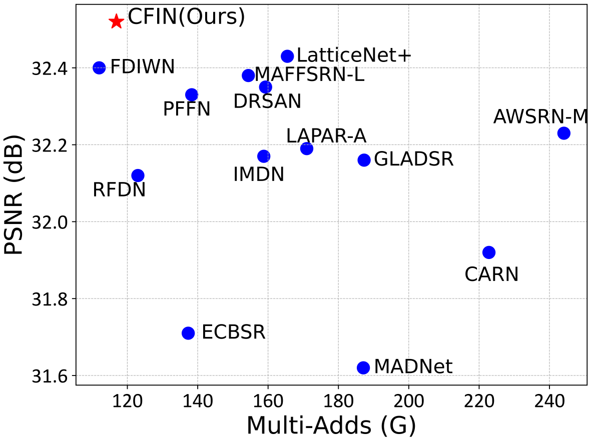

Fig. 9: Model performance and Multi-Adds comparison on Urban100 (×2). Obviously, our CFIN achieves the best balance between model performance and Multi-Adds.

B. *Complementarity of CNNs and Transformers*

CNN can be used to extract local features, and Transformer has powerful global modeling capabilities, both of which are crucial for high-quality image restoration. In TABLE X, we provide a comparison of CFIN with Pure-CNN and Pure-Transformer versions. Among them, Pure-CNN and Pure-Transformer represent variant models with only the CNN part or the Transformer part, respectively. For a fair comparison, the number of parameters of Pure-CNN is set as close to CFIN as possible, and the memory consumption of Pure-Transformer is set as close to CFIN as possible. It can be seen from the table that neither Pure-CNN nor Pure-Transformer cannot achieve the performance of the original CFIN. When using CNN alone, it can reduce the consumption of GPU memory, but it is difficult to improve the performance of the model even with more parameters. When using Transformer alone, the parameters of the model can be greatly reduced, but the consumption of GPU memory will rise rapidly, and its performance still hardly exceeds the original CFIN, which is not conducive to the practical application of the model. Therefore, we chose the hybrid model of CNN and Transformer, which can achieve a good balance between the size, GPU memory consumption, and performance of the model. Therefore, we can draw a conclusion that CNN and Transformer are complementary, and the combination of these two parts is feasible.

C. *Model Complexity Analysis*

We present the trade-off between our CFIN and other advanced SISR models in terms of PSNR, parameter amount, and inference time in Fig. 1. Obviously, CFIN attains the best performance among models with similar execution times and achieves the best balance in model complexity, inference time, and performance.

In Fig. 8 and Fig. 9, we also provide the parameter, Multi-Adds, and performance comparisons of CFIN with other advanced SISR models. It can be seen that our CFIN also achieved the best PSNR results under the premise of comparable calculations. Therefore, we can draw a conclusion that our CFIN is a lightweight and efficient model, which achieves the best balance between the model size and performance.

VI. Discussion

Although CFIN is an efficient model and achieve promising results, it still has some limitations and some details that need to pay attention:

(1) In this paper, we propose a lightweight and efficient CFIN for SISR. CFIN elegantly integrates CNN and Transformer, achieving competitive performance and a good balance between computational cost and performance. Different from the previous work [67], our CGA sent Q and K generated by the first CGA to the second CGA, and then add them with the new Q and K generated in the second CGA. After that, the result of the dot product of newly generated K and Q are dot products with V to obtain the final results. And the sizes of the kernel used in our two CGAs are different, thus these two modules have different receptive fields and can extract features with different scales. Therefore, through our method, features with different scales can be fused and guided with each other, which helps to make full use of image features to reconstruct more accurate images.

(2) We use some matrix multiplication in our model (especially matrix multiplication in CGA), so the training memory

is slightly larger. However, this does not mean the proposed method is meaningless. In summary, we proposed a new Transformer that can use modulated convolution kernel combined with locally representative semantic information to adaptively modify network weights, which can achieve excellent SR performance. We also note that some researchers [20] claimed that their methods can greatly reduce the memory required for Transformer training. In future works, We will further explore the effectiveness of these strategies and introduce them into CFIN to further improve the model.

VII. Conclusions

In this paper, we proposed a lightweight and efficient Cross-receptive Focused Inference Network (CFIN) for SISR. Specifically, we proposed a Cross-scale Information Aggregation Module (CIAM) composed of Redundant Information Filter Units (RIFUs) for filtering redundant information. Meanwhile, a Cross-receptive Field Guide Transformer (CFGT) is proposed for fine-grained information learning. In CFGT, Context Guided Max (CGM) is introduced to dynamically adjust the attention combined with neurons, and the cross-connection strategy is used to fuse context information across scales to meet the requirements of long-distance modeling. Extensive experiments have shown that CFIN can strike a good balance between the performance and complexity of the model.

References

[1] Y. Hu, J. Li, Y. Huang, and X. Gao, "Channel-wise and spatial feature modulation network for single image super-resolution," *IEEE Transactions on Circuits and Systems for Video Technology*, vol. 30, no. 11, pp. 3911–3927, 2020.

[2] Z.-S. Liu, W.-C. Siu, and Y.-L. Chan, "Photo-realistic image super-resolution via variational autoencoders," *IEEE Transactions on Circuits and Systems for video Technology*, vol. 31, no. 4, pp. 1351–1365, 2021.

[3] J. Zhang, C. Long, Y. Wang, H. Piao, H. Mei, X. Yang, and B. Yin, "A two-stage attentive network for single image super-resolution," *IEEE Transactions on Circuits and Systems for Video Technology*, vol. 32, no. 3, pp. 1020–1033, 2022.

[4] C. Dong, C. C. Loy, K. He, and X. Tang, "Image super-resolution using deep convolutional networks," *IEEE Transactions on Pattern Analysis and Machine Intelligence*, vol. 38, no. 2, pp. 295–307, 2015.

[5] M. Haris, G. Shakhnarovich, and N. Ukita, "Deep back-projection networks for super-resolution," in *CVPR*, 2018, pp. 1664–1673.

[6] Y. Zhang, Y. Tian, Y. Kong, B. Zhong, and Y. Fu, "Residual dense network for image super-resolution," in *CVPR*, 2018, pp. 2472–2481.

[7] X. Chu, B. Zhang, and R. Xu, "Multi-objective reinforced evolution in mobile neural architecture search," in *ECCV*, 2020, pp. 99–113.

[8] J. Li, F. Fang, K. Mei, and G. Zhang, "Multi-scale residual network for image super-resolution," in *ECCV*, 2018, pp. 517–532.

[9] J. Li, F. Fang, J. Li, K. Mei, and G. Zhang, "Mdcn: Multi-scale dense cross network for image super-resolution," *IEEE Transactions on Circuits and Systems for Video Technology*, vol. 31, no. 7, pp. 2547–2561, 2020.

[10] N. Ahn, B. Kang, and K.-A. Sohn, "Fast, accurate, and lightweight super-resolution with cascading residual network," in *ECCV*, 2018, pp. 252–268.

[11] Z. Wang, G. Gao, J. Li, Y. Yu, and H. Lu, "Lightweight image super-resolution with multi-scale feature interaction network," in *ICME*, 2021, pp. 1–6.

[12] N. Carion, F. Massa, G. Synnaeve, N. Usunier, A. Kirillov, and S. Zagoruyko, "End-to-end object detection with transformers," in *ECCV*, 2020, pp. 213–229.

[13] Z. Liu, Y. Lin, Y. Cao, H. Hu, Y. Wei, Z. Zhang, S. Lin, and B. Guo, "Swin transformer: Hierarchical vision transformer using shifted windows," in *ICCV*, 2021, pp. 10 012–10 022.

[14] H. Chen, Y. Wang, T. Guo, C. Xu, Y. Deng, Z. Liu, S. Ma, C. Xu, C. Xu, and W. Gao, "Pre-trained image processing transformer," in *CVPR*, 2021, pp. 12 299–12 310.

[15] R. Yu, D. Du, R. LaLonde, D. Davila, C. Funk, A. Hoogs, and B. Clipp, "Cascade transformers for end-to-end person search," in *CVPR*, June 2022, pp. 7267–7276.

[16] Z. Wang, X. Cun, J. Bao, W. Zhou, J. Liu, and H. Li, "Uformer: A general u-shaped transformer for image restoration," in *CVPR*, June 2022, pp. 17 683–17 693.

[17] G. Gao, Z. Wang, J. Li, W. Li, Y. Yu, and T. Zeng, "Lightweight bimodal network for single-image super-resolution via symmetric cnn and recursive transformer," *IJCAI*, 2022.

[18] X. Chen, X. Wang, J. Zhou, and C. Dong, "Activating more pixels in image super-resolution transformer," *arXiv preprint arXiv:2205.04437*, 2022.

[19] J. Liang, J. Cao, G. Sun, K. Zhang, L. Van Gool, and R. Timofte, "Swinir: Image restoration using swin transformer," in *ICCVW*, 2021, pp. 1833–1844.

[20] Z. Lu, J. Li, H. Liu, C. Huang, L. Zhang, and T. Zeng, "Transformer for single image super-resolution," in *CVPR Workshop*, 2022, pp. 457–466.

[21] C. D. Gilbert and W. Li, "Top-down influences on visual processing," *Nature Reviews Neuroscience*, vol. 14, no. 5, pp. 350–363, 2013.

[22] X. Jia, B. De Brabandere, T. Tuytelaars, and L. V. Gool, "Dynamic filter networks," in *NeurIPS*, 2016, pp. 20.1–29.9.

[23] Y. Chen, X. Dai, M. Liu, D. Chen, L. Yuan, and Z. Liu, "Dynamic convolution: Attention over convolution kernels," in *CVPR*, 2020, pp. 11 030–11 039.

[24] X. Lin, L. Ma, W. Liu, and S.-F. Chang, "Context-gated convolution," in *ECCV*, 2020, pp. 701–718.

[25] A. Lahiri, S. Bairagya, S. Bera, S. Haldar, and P. K. Biswas, "Lightweight modules for efficient deep learning based image restoration," *IEEE Transactions on Circuits and Systems for Video Technology*, vol. 31, no. 4, pp. 1395–1410, 2021.

[26] R. Lan, L. Sun, Z. Liu, H. Lu, C. Pang, and X. Luo, "Madnet: a fast and lightweight network for single-image super resolution," *IEEE Transactions on Cybernetics*, vol. 51, no. 3, pp. 1443–1453, 2020.

[27] X. Zhang, P. Gao, S. Liu, K. Zhao, G. Li, L. Yin, and C. W. Chen, "Accurate and efficient image super-resolution via global-local adjusting dense network," *IEEE Transactions on Multimedia*, vol. 23, pp. 1924–1937, 2021.

[28] L. Wang, X. Dong, Y. Wang, X. Ying, Z. Lin, W. An, and Y. Guo, "Exploring sparsity in image super-resolution for efficient inference," in *CVPR*, 2021, pp. 4917–4926.

[29] D. Zhang, C. Li, N. Xie, G. Wang, and J. Shao, "Pffn: Progressive feature fusion network for lightweight image super-resolution," in *ACMMM*, 2021, pp. 3682–3690.

[30] K. Park, J. W. Soh, and N. I. Cho, "Dynamic residual self-attention network for lightweight single image super-resolution," *IEEE Transactions on Multimedia*, 2021.

[31] X. Zhu, K. Guo, S. Ren, B. Hu, M. Hu, and H. Fang, "Lightweight image super-resolution with expectation-maximization attention mechanism," *IEEE Transactions on Circuits and Systems for Video Technology*, vol. 32, no. 3, pp. 1273–1284, 2022.

[32] Z. Hui, X. Wang, and X. Gao, "Fast and accurate single image super-resolution via information distillation network," in *CVPR*, 2018, pp. 723–731.

[33] Z. Hui, X. Gao, Y. Yang, and X. Wang, "Lightweight image super-resolution with information multi-distillation network," in *ACMMM*, 2019, pp. 2024–2032.

[34] J. Liu, J. Tang, and G. Wu, "Residual feature distillation network for lightweight image super-resolution," in *ECCV*, 2020, pp. 41–55.

[35] X. Jiang, N. Wang, J. Xin, X. Xia, X. Yang, and X. Gao, "Learning lightweight super-resolution networks with weight pruning," *Neural Networks*, vol. 144, pp. 21–32, 2021.

[36] G. Gao, W. Li, J. Li, F. Wu, H. Lu, and Y. Yu, "Feature distillation interaction weighting network for lightweight image super-resolution," *arXiv preprint arXiv:2112.08655*, 2021.

[37] J. Hu, L. Shen, and G. Sun, "Squeeze-and-excitation networks," in *CVPR*, 2018, pp. 7132–7141.

[38] F. Wu, A. Fan, A. Baevski, Y. N. Dauphin, and M. Auli, "Pay less attention with lightweight and dynamic convolutions," *arXiv preprint arXiv:1901.10430*, 2019.

[39] X. Zhu, H. Hu, S. Lin, and J. Dai, "Deformable convnets v2: More deformable, better results," in *CVPR*, 2019, pp. 9308–9316.

[40] Y. Jo, S. W. Oh, J. Kang, and S. J. Kim, "Deep video super-resolution network using dynamic upsampling filters without explicit motion compensation," in *CVPR*, 2018, pp. 3224–3232.

[41] Y. Yang, Z. Zhong, T. Shen, and Z. Lin, "Convolutional neural networks with alternately updated clique," in *CVPR*, 2018, pp. 2413–2422.

[42] C. Xie, Y. Wu, L. v. d. Maaten, A. L. Yuille, and K. He, "Feature denoising for improving adversarial robustness," in *CVPR*, 2019, pp. 501–509.

[43] R. Zhang, "Making convolutional networks shift-invariant again," in *ICML*, 2019, pp. 7324–7334.

[44] S. A. Magid, Y. Zhang, D. Wei, W.-D. Jang, Z. Lin, Y. Fu, and H. Pfister, "Dynamic high-pass filtering and multi-spectral attention for image super-resolution," in *ICCV*, 2021, pp. 4288–4297.

[45] E. Jang, S. Gu, and B. Poole, "Categorical reparameterization with gumbel-softmax," *arXiv preprint arXiv:1611.01144*, 2016.

[46] A. Vaswani, N. Shazeer, N. Parmar, J. Uszkoreit, L. Jones, A. N. Gomez, Ł. Kaiser, and I. Polosukhin, "Attention is all you need," in *NeurIPS*, 2017, pp. 30.1–30.11.

[47] A. Dosovitskiy, L. Beyer, A. Kolesnikov, D. Weissenborn, X. Zhai, T. Unterthiner, M. Dehghani, M. Minderer, G. Heigold, S. Gelly *et al.*, "An image is worth 16x16 words: Transformers for image recognition at scale," *arXiv preprint arXiv:2010.11929*, 2020.

[48] X. Chen, L.-J. Li, L. Fei-Fei, and A. Gupta, "Iterative visual reasoning beyond convolutions," in *CVPR*, 2018, pp. 7239–7248.

[49] K. Li, Y. Zhang, K. Li, Y. Li, and Y. Fu, "Visual semantic reasoning for image-text matching," in *ICCV*, 2019, pp. 4654–4662.

[50] Y. Tai, J. Yang, and X. Liu, "Image super-resolution via deep recursive residual network," in *CVPR*, 2017, pp. 3147–3155.

[51] C. Wang, Z. Li, and J. Shi, "Lightweight image super-resolution with adaptive weighted learning network," *arXiv preprint arXiv:1904.02358*, 2019.

[52] A. Muqeet, J. Hwang, S. Yang, J. Kang, Y. Kim, and S.-H. Bae, "Multi-attention based ultra lightweight image super-resolution," in *ECCV*, 2020, pp. 103–118.

[53] W. Li, K. Zhou, L. Qi, N. Jiang, J. Lu, and J. Jia, "Lapar: Linearly-assembled pixel-adaptive regression network for single image super-resolution and beyond," in *NeurIPS*, 2020, pp. 20 343–20 355.

[54] X. Luo, Y. Xie, Y. Zhang, Y. Qu, C. Li, and Y. Fu, "Latticenet: Towards lightweight image super-resolution with lattice block," in *ECCV*, 2020, pp. 272–289.

[55] Y. Li, J. Cao, Z. Li, S. Oh, and N. Komuro, "Lightweight single image super-resolution with dense connection distillation network," *ACM TOMM*, vol. 17, no. 1s, pp. 1–17, 2021.

[56] X. Zhang, H. Zeng, and L. Zhang, "Edge-oriented convolution block for real-time super resolution on mobile devices," in *ACMMM*, 2021, pp. 4034–4043.

[57] R. Timofte, E. Agustsson, L. Van Gool, M.-H. Yang, and L. Zhang, "Ntire 2017 challenge on single image super-resolution: Methods and results," in *CVPRW*, 2017, pp. 114–125.

[58] M. Bevilacqua, A. Roumy, C. Guillemot, and M. L. Alberi-Morel, "Low-complexity single-image super-resolution based on nonnegative neighbor embedding," in *BMVC*, 2012, pp. 135.1–135.10.

[59] R. Zeyde, M. Elad, and M. Protter, "On single image scale-up using sparse-representations," in *ICCS*, 2010, pp. 711–730.

[60] D. Martin, C. Fowlkes, D. Tal, and J. Malik, "A database of human segmented natural images and its application to evaluating segmentation algorithms and measuring ecological statistics," in *ICCV*, 2001, pp. 416–423.

[61] J.-B. Huang, A. Singh, and N. Ahuja, "Single image super-resolution from transformed self-exemplars," in *CVPR*, 2015, pp. 5197–5206.

[62] Y. Matsui, K. Ito, Y. Aramaki, A. Fujimoto, T. Ogawa, T. Yamasaki, and K. Aizawa, "Sketch-based manga retrieval using manga109 dataset," *Multimedia Tools and Applications*, vol. 76, no. 20, pp. 21 811–21 838, 2017.

[63] T. Salimans and D. P. Kingma, "Weight normalization: A simple reparameterization to accelerate training of deep neural networks," in *NeurIPS*, 2016, pp. 29.1–29.9.

[64] B. Lim, S. Son, H. Kim, S. Nah, and K. Mu Lee, "Enhanced deep residual networks for single image super-resolution," in *CVPRW*, 2017, pp. 136–144.

[65] Y. Zhang, K. Li, K. Li, L. Wang, B. Zhong, and Y. Fu, "Image super-resolution using very deep residual channel attention networks," in *ECCV*, 2018, pp. 286–301.

[66] H. Zhao, X. Kong, J. He, Y. Qiao, and C. Dong, "Efficient image super-resolution using pixel attention," in *ECCVW*, 2020, pp. 56–72.

[67] R. Song, W. Ni, W. Cheng, and X. Wang, "Csanet: Cross-temporal interaction symmetric attention network for hyperspectral image change detection," *IEEE Geoscience and Remote Sensing Letters*, 2022.